# A spatial constraint to model and extract texture components in Multivariate Curve Resolution of near-infrared hyperspectral images

Raffaele Vitale, Siewert Hugelier, Dario Cevoli, Cyril Ruckebusch

Version of Record: https://www.sciencedirect.com/science/article/pii/S0003267019312383
Manuscript_5f1ace0c7f943458ecc5224a74ed4d5e

# A spatial constraint to model and extract texture components in Multivariate Curve Resolution of near-infrared hyperspectral images

Raffaele Vitale[a,b,*], Siewert Hugelier[a], Dario Cevoli[a], Cyril Ruckebusch[a]

[a]*Laboratoire de Spectrochimie Infrarouge et Raman - LASIR CNRS - UMR 8516, Université de Lille, Bâtiment C5, F-59000, Lille, France*
[b]*Molecular Imaging and Photonics Unit, Department of Chemistry, Katholieke Universiteit Leuven, Celestijnenlaan 200F, B-3001, Leuven, Belgium*

**Abstract**

This article highlights the importance of properly taking into account spatial structures and features to better resolve near-infrared (NIR) hyperspectral images by Multivariate Curve Resolution-Alternating Least Squares (MCR-ALS), especially when highly mixed components (in terms of spatial and spectral overlap) underlying the systems under study are dealt with. As in the NIR domain these components can explain both chemical properties and physical phenomena, their improved unravelling can therefore represent an alternative or a complement to more standard approaches for, *e.g.*, spectral data preprocessing. These points will be illustrated through the comprehensive analysis of a complex real-world forensic case-study where texture characterization is crucial for the sake of a more appropriate resolution.

*Keywords:* Multivariate Curve Resolution-Alternating Least Squares (MCR-ALS), near-infrared (NIR) hyperspectral images, spatial constraints, texture extraction, forensics

## 1. Introduction

Over the last two decades, the development and diffusion of hyperspectral imaging devices has led to significant advances in many scientific and technological fields, like microscopy, geoscience and biomedicine [1–3]. Compared to classical RGB imaging, in which light intensity is recorded only in correspondence of the red, green and blue color channels, hyperspectral imaging allows users to register full spectra (within specific wavelength ranges) for every scanned pixel of the sample under study, enabling the collection of complex and comprehensive information about the spatial distribution of the various chemical constituents of its surface.
Usually, and especially if hyperspectral images are utilized for calibration or classification purposes, data preprocessing represents a crucial step for the linearization of the instrumental response

*Corresponding author:
*Telephone number:* +33769476654 ext. 74935
*Email address:* rvitale86@gmail.com (Raffaele Vitale)

and for the subsequent extraction of valuable and meaningful information about the investigated objects [4]. Preprocessing generally aims at filtering out irrelevant or unwanted variation from the collected signal. Most of this variation is usually due to the physical properties of the target scene and may yield significant changes or distortions of the acquired spectral profiles. As an example, in the near-infrared (NIR) domain, light scattering resulting from, *e.g.*, the texture of a fabric tissue commonly generates a typical additive/multiplicative baseline effect which can mask chemical features of interest [5]. However, correcting for such effects is not straightforward since the choice of the most suitable spectral pretreatment approach mainly relies on the expertise of the analyst, trial and error, and can be heavily biased [6]. Furthermore, in many situations, *a priori* information on the morphology of the analyzed sample is not available or can hardly be translated into a series of mathematical operations to be performed on the spectra. In similar scenarios one may be interested in modelling all possible sources of variation (*components* or *factors*) underlying the hyperspectral measurements without preliminarily removing those that in principle are uninteresting and/or undesired. In order to unravel the single contributions associated to such components, practitioners commonly resort to Multivariate Curve Resolution (MCR) approaches (also classified by the more general definition of *spectral unmixing* techniques in the domain of remote sensing) [7]. In general, MCR methodologies permit to retrieve the spectral fingerprint of each one of these components and their distribution in space across the imaged region, provided the concerned data follow a bilinear mathematical model. Nevertheless, most of these approaches (or at least those well-established in chemometrics) suffer from a particular limitation: as hyperspectral images are characterized by a three-dimensional data structure (of dimensions $N_x \times N_y \times J$, where $N_x$ is the number of pixels in the $x$-dimension, $N_y$ the number of pixels in the $y$-dimension and $J$ the number of sampled wavelengths), their analysis can usually be carried out only if they are preliminarily unfolded into a matrix whose rows contain the spectra recorded for all the pixels under study. Unfortunately, through this unfolding procedure, the spatial information (*i.e.* the degree of correlation, similarity of dissimilarity among neighbouring pixels) is inevitably lost and cannot be directly exploited for obtaining more meaningful descriptions of the system at hand. However, spatial information is a core aspect of a hyperspectral image and neglecting it boils down to considering only one side of the coin [8–14]. In addition, as here the data decomposition is only driven by the nature of the spectra collected by the imaging equipment, profile distortions like the ones mentioned before could easily worsen its quality.

In the light of all these aspects, this article will show how integrating and employing spatial information in the framework of MCR methods (and concretely of Multivariate Curve Resolution-Alternating Least Squares - MCR-ALS [15, 16]) can lead to a better resolution of NIR hyperspectral images especially when dealing with highly mixed components. As such components can be associated to both chemical properties and physical phenomena, their improved disentanglement might therefore represent an alternative or a complement to more standard approaches for spectral data preprocessing. These points will be illustrated through the comprehensive analysis of a complex real-world case-study where texture isolation is pivotal for the sake of a more appropriate resolution.

## 2. Materials and methods

### *2.1. Multivariate Curve Resolution-Alternating Least Squares (MCR-ALS)*

In analytical chemistry and chemometrics, spectral unmixing is usually achieved by MCR-ALS [15, 16], which, differently from geometrical techniques (rather popular in the field of remote sensing), is more indicated when highly overlapping signal contributions need to be unravelled. MCR-ALS is a standard soft-modelling approach initially developed for the resolution of multi-component evolving chemical systems which solves the following bilinear additive model based on the Lambert-Beer law:

$$\mathbf{D} = \mathbf{C}\mathbf{S}^{\mathrm{T}} + \mathbf{E} \tag{1}$$

The goal of this method is the decomposition of the matrix $\mathbf{D}$ (say $N \times J$) into the profiles $\mathbf{C}$ ($N \times A$) and $\mathbf{S}^{\mathrm{T}}$ ($A \times J$) associated to the data variation along its rows and columns, respectively, and, thus, usually reflecting the concentration (or abundance) and the pure spectral fingerprint of the resolved constituents of the investigated samples. $\mathbf{E}$ ($N \times J$) denotes the residuals array, *i.e.*, the portion of $\mathbf{D}$ not explained at the chosen rank, $A$ (generally estimated by inspecting the singular values of $\mathbf{D}$ [15]). MCR-ALS iteratively solves Equation 1 by alternately calculating $\mathbf{C}$ and $\mathbf{S}^{\mathrm{T}}$, optimally fitting the experimental data matrix $\mathbf{D}$ and minimizing the so-called lack-of-fit ($LOF$) expressed as:

$$LOF(\%) = 100\sqrt{\frac{\sum_{n,j} e_{n,j}}{\sum_{n,j} d_{n,j}}} \tag{2}$$

with $e_{n,j}$ and $d_{n,j}$ being the $(n \times j)$-th element of $\mathbf{E}$ and $\mathbf{D}$, respectively. Such an optimization is carried out for a certain number of components and exploiting initial guesses of either $\mathbf{C}$ or $\mathbf{S}^{\mathrm{T}}$, computed *e.g.* based on a preliminary knowledge of the system under study, by Evolving Factor Analysis (EFA) [17], SIMPLe-to-use Interactive Self-modeling Mixture Analysis (SIMPLISMA) [18] or derived methods. In any case, specific constraints to $\mathbf{C}$ and/or $\mathbf{S}^{\mathrm{T}}$ (*e.g.*, non-negativity) are to be applied in order to restrict the MCR-ALS solution, reduce its ambiguity (see also Ref. [19, 20] for a more detailed definition of MCR-ALS solution ambiguity) and obtain meaningful response profiles from a physicochemical point of view. It goes without saying that in several circumstances pretreatment operations like spectral derivations might be incompatible with the nature of such constraints.

### *2.2. MCR-ALS of hyperspectral data*

When MCR-ALS is to be applied to hyperspectral imaging data, its algorithmic procedure starts with a preliminary unfolding of the three-dimensional structure of the hyperspectral image ($N_x \times N_y \times J$) into the matrix $\mathbf{D}$ (now, of size $N_x N_y \times J$), whose rows contain the various spectral profiles recorded for the different sampled pixels (see also Section 1). It is this matrix that is afterwards decomposed as explained in Section 2.1. Potential information related to the spatial correlation or similarity among neighbouring pixels can be exploited in MCR-ALS by applying image processing constraints as recently proposed in Ref. [8]. In other words, specific spatial structures or features are imposed for the distribution of the different resolved components within the image. By this approach, at each ALS iteration the single column vectors of $\mathbf{C}$ are refolded into *temporary* component distribution maps. These temporary distribution maps can be at this point

subjected to any classical image processing algorithm and finally unfolded again for allowing the computational procedure to progress. As one can easily envision, all types of greyscale image processing tools can be, in principle, directly used on the single temporary distribution maps *during* the MCR-ALS optimization as proper constraints to impose specific spatial features on the profiles in **C**. These spatial features can be different among components (*i.e.* different temporary distribution maps can be subjected to different image processing constraints), which makes this methodology particularly flexible for handling even very complex real case-studies and superior to processing the entire set of hyperspectral data in the same way. This adaptation of the classical MCR-ALS algorithm has proven to enable reliable and robust resolutions of hyperspectral images [8–14].

### *2.3. Relative Total Variation (RTV) constraint*

The spatial constraint implemented for this work is based on the concept of Relative Total Variation (RTV). RTV is a local smoothing operator first proposed for texture removal in grayscale and RGB images which solves the following objective function:

$$\arg\min_{\mathbf{I}_{\text{out}}} \sum_{p} (\mathbf{I}_{\text{out},p} - \mathbf{I}_{\text{in},p})^2 + \lambda \left( \frac{\mathfrak{D}_x(p)}{\mathfrak{L}_x(p) + \epsilon} + \frac{\mathfrak{D}_y(p)}{\mathfrak{L}_y(p) + \epsilon} \right) \tag{3}$$

where the index $p$ denotes an image window centered at pixel $p$, $\mathbf{I}_{\text{out},p}$ and $\mathbf{I}_{\text{in},p}$ are the output (processed) and the input (measured) image windows centered at pixel $p$, respectively, $\lambda$ is a regularization parameter controlling the weight of the penalty term of Equation 3 during the computational procedure, $\mathfrak{D}_x(p)/\mathfrak{D}_y(p)$ measures the intensity gradient in the $x$-/$y$-direction within the rectangular image window centered at pixel $p$, $\mathfrak{L}_x(p)/\mathfrak{L}_y(p)$ captures the overall spatial intensity variation along the $x$-/$y$-direction within the rectangular image window centered at pixel $p$, and $\epsilon$ is a small positive number to avoid division by 0. Interested readers are addressed to Ref. [21] for a good survey about the mathematical details of the original methodology. RTV exploits the principles of the Total Variation (TV) algorithm developed by Rudin *et al.* [22], but locally. Nevertheless, it is important to highlight that if TV is able to filter high-frequency intensity variation out of the images at hand while preserving boundaries separating different objects or Regions Of Interest (ROIs), it features a limited ability to distinguish strong structural edges and textures. On the other hand, RTV enhances contrast between these two elements and yields a more effective structure-texture decomposition. More concretely, textural information can be recovered by calculating the difference between the input image and its RTV-smoothed version (*inverse* RTV).
RTV also requires the optimization of $\lambda$ in order to regulate the degree of smoothing. Finding a univocal criterion for assessing the smoothing quality is not straightforward, making an automatic adjustment difficult. Here, as also suggested in [12], $\lambda$ is manually tuned outside the ALS loop and for every individual component distribution map resulting from a first spatially unconstrained MCR-ALS analysis. It is then kept fixed when RTV is subsequently applied to each column of **C** after refolding (see Section 2.2) during a spatially constrained MCR-ALS decomposition.

### *2.4. Dataset*

The main object of this study is a $239 \times 185$-sized NIR hyperspectral image of a white cotton sample onto which a drop of human semen has been deposited. This image (firstly described in

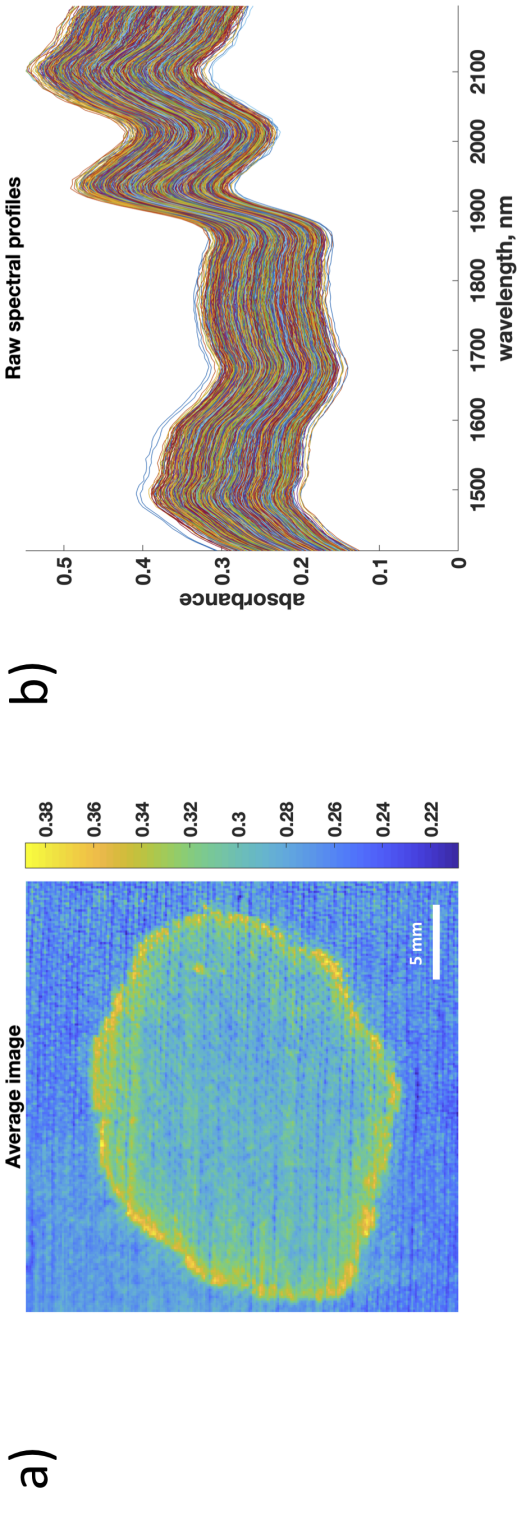


Figure 1 – Cotton/semen data - a) wavelength-wise average image (the semen stain is clearly visible in the middle) and b) raw spectral profiles

[23]) was originally collected by a Specim SisuCHEMA Short Wave InfraRed (SWIR) imaging equipment (spectral resolution: 10 nm; pixel size: $156 \times 156\ \mu m^2$; 50 mm lens) in the wavelength range between 1412 and 2194 nm in the attempt of extracting a spectral profile as specific as possible for the semen component which could be ideally utilized for forensic matching procedures. As highlighted in Figure 1, the data are characterized by an extremely high degree of spatial and spectral overlap. Chemical and physical information are heavily mixed which will dramatically jeopardize the correct retrieval of the pure distribution maps and spectral profiles of the different components underlying the system at hand. Two additional image datasets resulting from similar deposition experiments, acquired through the same instrumentation and of dimensions $222 \times 210$ and $247 \times 215$, respectively, will also be exploited for the assessment of the reliability of the MCR-ALS solutions that will be reported in the following sections.

## 3. Results and discussion

### *3.1. Estimate of the number of components, A*

In order to get an idea about the number of components underlying the cotton/semen image, both a global and a local rank analysis were carried out by Singular Value Decomposition (SVD - as detailed in Section 2.1) and Fixed Size Image Window-Evolving Factor Analysis (FSIW-EFA) [24, 25], respectively. Figure 2 shows the resulting eigenvalue plot and local rank map. Each pixel of the local rank map is colored according to the number of pure components contributing to the signal variation of the corresponding original spectrum. As one can clearly see, no pure pixels can be found (*i.e.*, every spectrum of the hyperspectral image is supposed to originate from the combination or mixture of at least 2 different components) which corroborates what was detailed in Section 2.4 regarding the complexity of the concerned case-study. Based on the displayed outcomes, $A$ was set equal to 5 for subsequent MCR-ALS modelling.

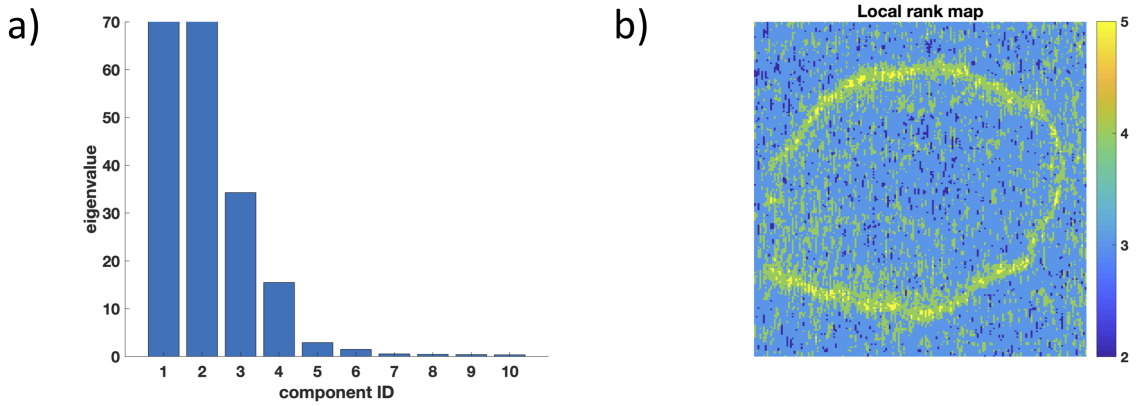


Figure 2 – Cotton/semen data - a) Eigenvalue plot and b) local rank map for an image window of dimensions $3 \times 3$. Each pixel of the local map is colored according to the number of pure components contributing to the signal variation of the corresponding spectrum. Notice that the spectral information of some of the pixels along the borders of the image is lost during local rank estimation. For this reason, its original dimensions do not exactly match the size of the represented map. The $y$-scale in a) was adapted for highlighting smaller eigenvalues

### *3.2. MCR-ALS with non-negativity constraint*

A first MCR-ALS decomposition was performed starting from an estimation of $\mathbf{S}^T$ yielded by SIMPLISMA and imposing only a non-negativity constraint on $\mathbf{C}$ and $\mathbf{S}^T$ (see Section 2.1). It is important to notice here that partially constrained MCR-ALS models can conform better with the nature of the original data and provide good initial estimates for more or fully constrained ones. The resolution obtained (exhibiting a particularly satisfactory *LOF* of 0.5%) is represented in Figure 3. A rather adequate discrimination among the different regions of interest of the image is achieved: i) the first three components roughly separate semen, fabric texture and cotton contributions (see Figures 3a, 3b, 3c, 3g, 3h and 3i); ii) a fourth component (see Figures 3d and 3j) probably reflects an effect associated to the border of the dried semen stain resulting in a spectral offset; iii) an additional component (see Figures 3e and 3k) highlights a pattern related to the diffusion of the semen drop across the area of the stain. However, from Figure 3, it is also evident how the extracted concentration distribution maps of the five components are anyway characterized by a spurious contribution associated to the texture of the cotton support. This indicates that the disentanglement of the various components is not perfect and that the extracted spectral profiles (especially the one of interest - the semen spectral profile, see Figure 3b) might not be specific. Therefore, RTV was implemented as texture extraction constraint in the MCR-ALS framework outlined in Section 2.2 in the attempt of improving both spatial and spectral selectivity.

### *3.3. MCR-ALS with non-negativity and RTV constraints*

The resolution obtained by performing an MCR-ALS decomposition imposing non-negativity on $\mathbf{C}$ and $\mathbf{S}^T$ and RTV on the temporary distribution maps of components #1, #2, #3 and #5 (see Section 2.2) is represented in Figure 4. Notice that in this case no spatial constraint was applied to component #4. Moreover, the temporary distribution map of component #2 was computed as the difference between the one resulting from the ALS algorithmic procedure and its RTV-smoothed version (see Section 2.3). This permits to achieve a finer visual isolation of the two distribution maps and spectral profiles affected by scattering phenomena (see Figures 4b and 4h and Figures 4d and 4j), while preserving the ROI boundary between semen and pure cotton.
Somehow, with respect to what was shown in the previous section, Figure 4 highlights the presence of three components accounting for the semen (#1), cotton (#3) and semen gradient (#5) contribution, and two components (#2, #4) basically explaining a wavelength dependent and an approximately additive offset effect, respectively (see Figures 4h and 4j). To corroborate this point, an additional MCR-ALS decomposition of the same hyperspectral image after first-derivative transformation [26] of its original spectral profiles was produced (see Figure 5). Here, four components were sufficient to account for 99.7% of the data variability and, as one can easily see, together with a better spatial separation of the cotton fabric texture (see Figure 5b), the suppression of the aforementioned offset effect was achieved. This is reasonable if one thinks that spectral derivation allows additive baseline contributions to be completely removed. The same is not valid for the wavelength dependent effect, likely related (at least partly) to optical Rayleigh scattering and whose elimination may require more elaborated preprocessing approaches. The readers can refer to the Supporting Information of this article for the outcomes returned by the MCR-ALS analysis

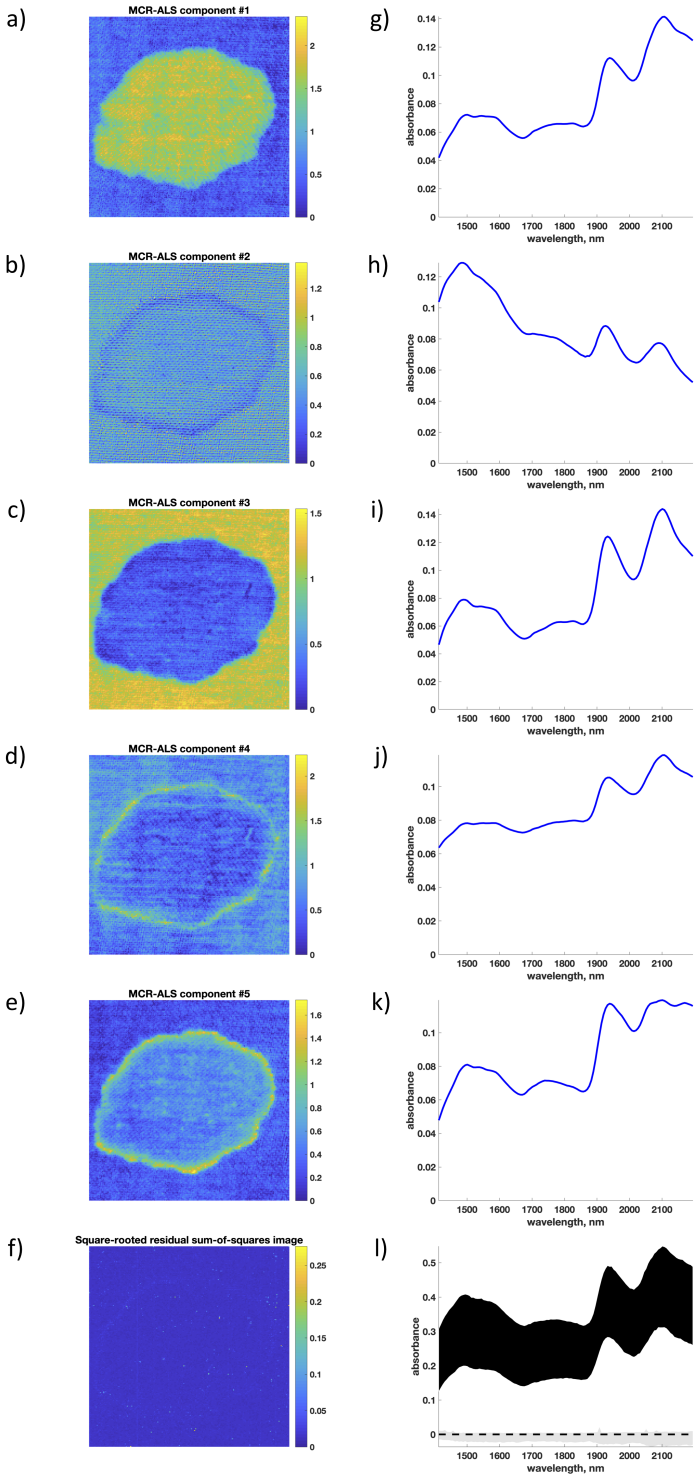


Figure 3 – Cotton/semen data - a)-e) Component distribution maps and g)-k) resolved spectral profiles obtained by performing a standard MCR-ALS decomposition (see Section 2.1) imposing a non-negativity constraint on both $\mathbf{C}$ and $\mathbf{S}^{\mathrm{T}}$. $LOF = 0.5\%$. f) Square-rooted residual sum-of-squares image. l) Representation of the spectral area spanned by the raw data (black) and by the MCR-ALS residuals (gray), respectively

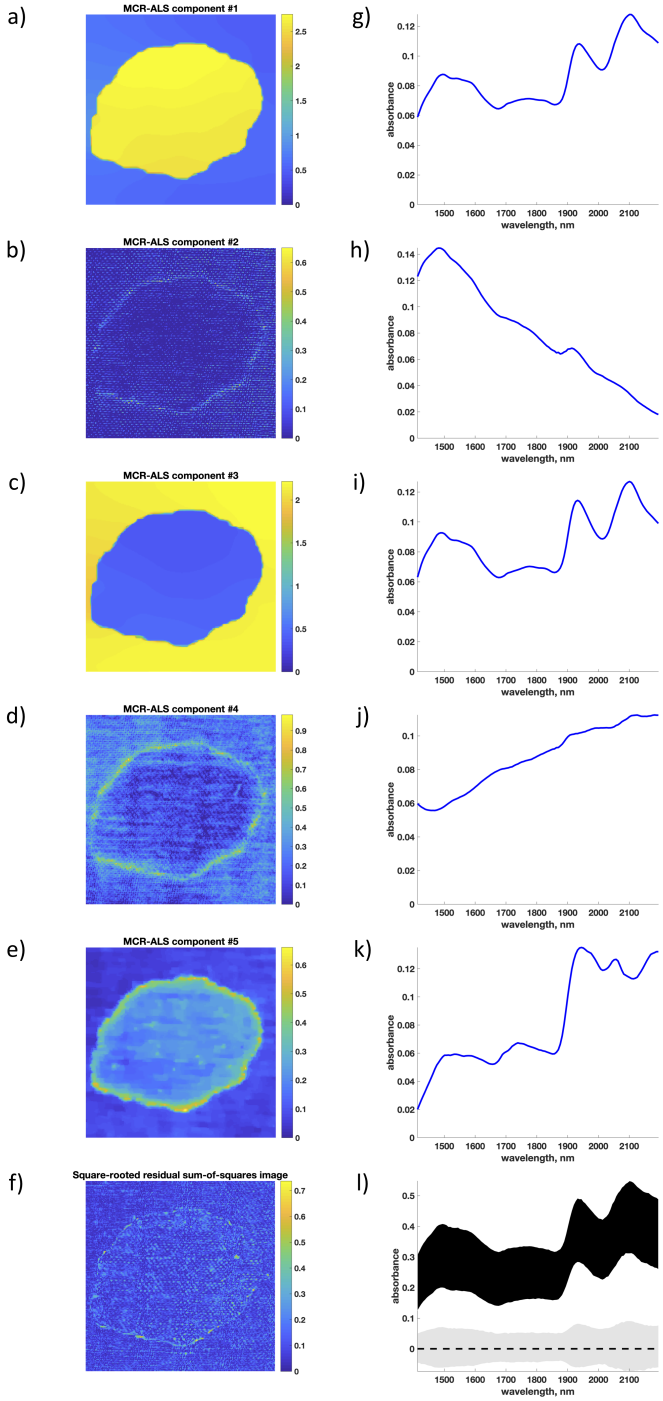


Figure 4 – Cotton/semen data - a)-e) Component distribution maps and g)-k) resolved spectral profiles obtained by performing an MCR-ALS decomposition (see Section 2.2) imposing a non-negativity constraint on both $\mathbf{C}$ and $\mathbf{S}^{\mathrm{T}}$ and an RTV constraint on the temporary $\mathbf{C}$ refolded vectors associated to factors #1, #2, #3 and #5 ($\lambda_1 = 0.055$, $\lambda_2 = 0.65$, $\lambda_3 = 0.07$, $\lambda_5 = 0.00225$, where $\lambda_a$ denotes the $\lambda$ parameter value imposed for the RTV smoothing of the $a$-th MCR-ALS component distribution map). As described in Section 2.3, RTV was applied in an *inverse* fashion for component #2. $LOF = 3.9\%$. f) Square-rooted residual sum-of-squares image. l) Representation of the spectral area spanned by the raw data (black) and by the MCR-ALS residuals (gray), respectively

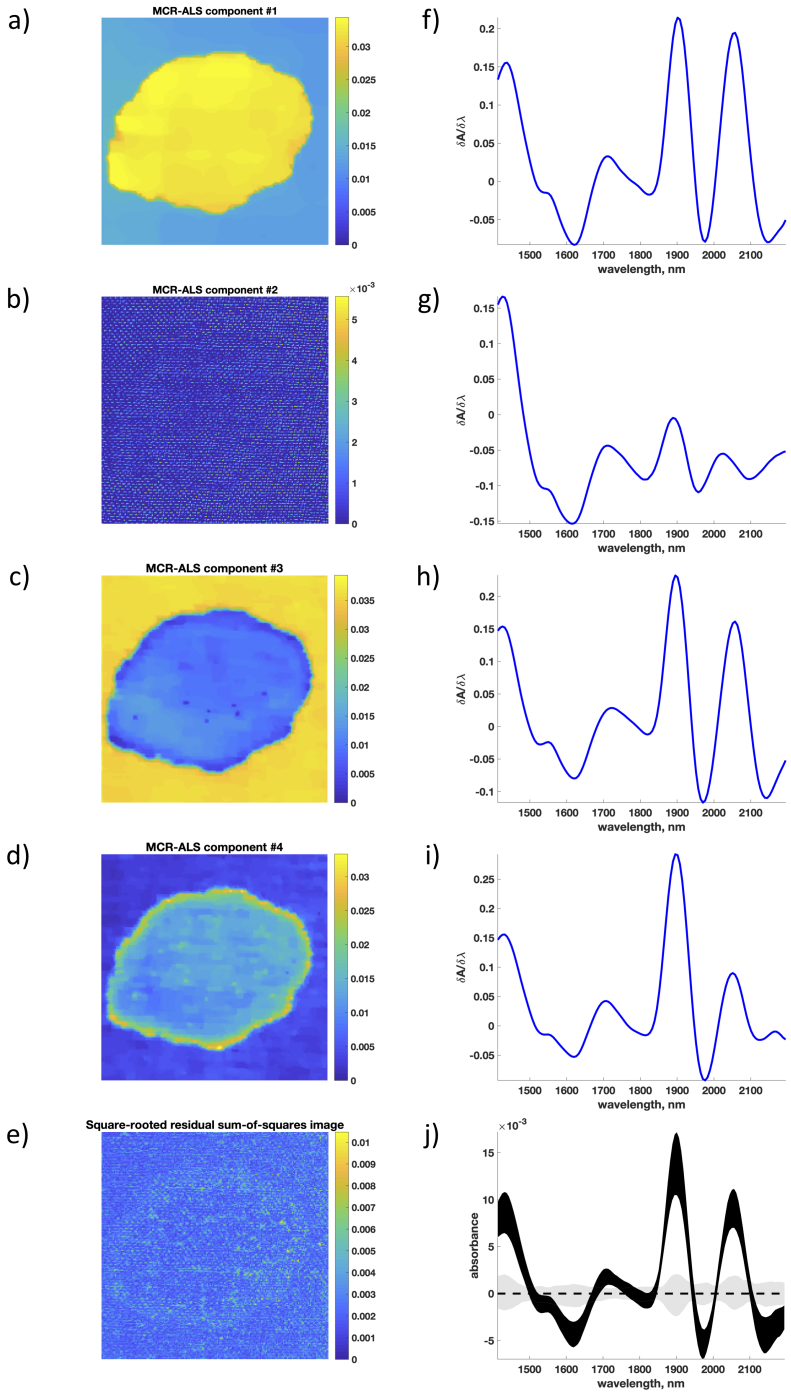


Figure 5 – Cotton/semen first-derivative data - a)-d) Component distribution maps and f)-i) resolved spectral profiles obtained by performing an MCR-ALS decomposition (see Section 2.2) imposing a non-negativity constraint on **C** and an RTV constraint on the temporary **C** refolded vectors associated to factors #1, #2, #3 and #4 ($\lambda_1 = 0.009$, $\lambda_2 = 0.005$, $\lambda_3 = 0.004$, $\lambda_5 = 0.002$, where $\lambda_a$ denotes the $\lambda$ parameter value imposed for the RTV smoothing of the $a$-th MCR-ALS component distribution map). As described in Section 2.3, RTV was applied in an *inverse* fashion for component #2. $LOF = 5.1\%$. e) Square-rooted residual sum-of-squares image. j) Representation of the spectral area spanned by the raw data (black) and by the MCR-ALS residuals (gray), respectively

of second-order derivative data[i]. However, at least from an illustrative point of view, it is clear how coupling MCR-ALS and spatial constraints may lead to a more performant discrimination of physical and chemical phenomena affecting hyperspectral data (which, in a certain sense, is often the aim of data preprocessing techniques) and enable a better description of systems characterized by a high degree of complexity (in terms of spatial and spectral overlap among components).

### *3.4. Reliability of the MCR-ALS decomposition*

Two additional hyperspectral images of the same type of sample collected within the same wavelength range were also analyzed in order to evaluate the reliability and robustness of the MCR-ALS solutions yielded by the two different strategies outlined in Sections 2.1 and 2.2. The resolved spectral profiles resulting from the decomposition of the data are displayed in Figure 6. Component distributions maps and *LOF* values (not shown) were found to be in close agreement with those shown before (see Section 3.3). From Figure 6, it is evident that applying standard MCR-ALS simply imposing a non-negativity constraint on $\mathbf{C}$ returns rather variable spectral fingerprints to be unravelled (especially concerning the first three components - see Figures 6a-c), which might jeopardize their direct exploitation for forensic matching procedures. Conversely, when RTV is utilized as an extra spatial constraint, such a variability is significantly reduced, in particular for the semen component which is the one of greatest interest (see Figures 6a and 6f).

## 4. Conclusions

In this paper, some of the striking advantages of constraining spatial features and structures in the analysis of hyperspectral images by MCR-ALS were highlighted throughout a complex forensic case-study. Apart from yielding a better description of the considered systems, this enabled an improved disentanglement of the chemical and physical events or phenomena affecting the analyzed datasets (*e.g.*, absorption, scattering, reflection, *etc*.), allowing specific sources of variability to be more precisely isolated and, possibly, filtered out. Such an improved disentanglement can therefore represent an alternative or a complement to more standard approaches for spectral data pretreatment, which usually require a high degree of expertise or *a priori* knowledge and can generate heavily biased outcomes if not applied properly. In fact, in the presence of strong light scattering as for the data investigated here, the linear MCR-ALS model may sometimes not be fulfilled since single pixels might be underlain by component co-occurrence and/or interaction. In such situations, characterizing the spatial factors which originate from the scattering phenomena (provided these factors are actually structured) could constitute a more reliable solution than spectral preprocessing. In this work, it was shown how an MCR-ALS model can approximate mixtures of highly overlapping components (both in space and along the wavelength range under study) with a good degree of confidence. The use of an RTV-based constraint resulted in a robust and more reliable resolution of these components, whose spatial contributions were forced to follow either smooth or more variable and irregular patterns. As a consequence of this, reproducible

[i]Second-order derivation reduces the global rank of the data to 3 and yields the loss of the gradient component. Yet, the textural effect is not completely filtered out, and still better isolated from the other two components under study when the RTV constraint is applied.

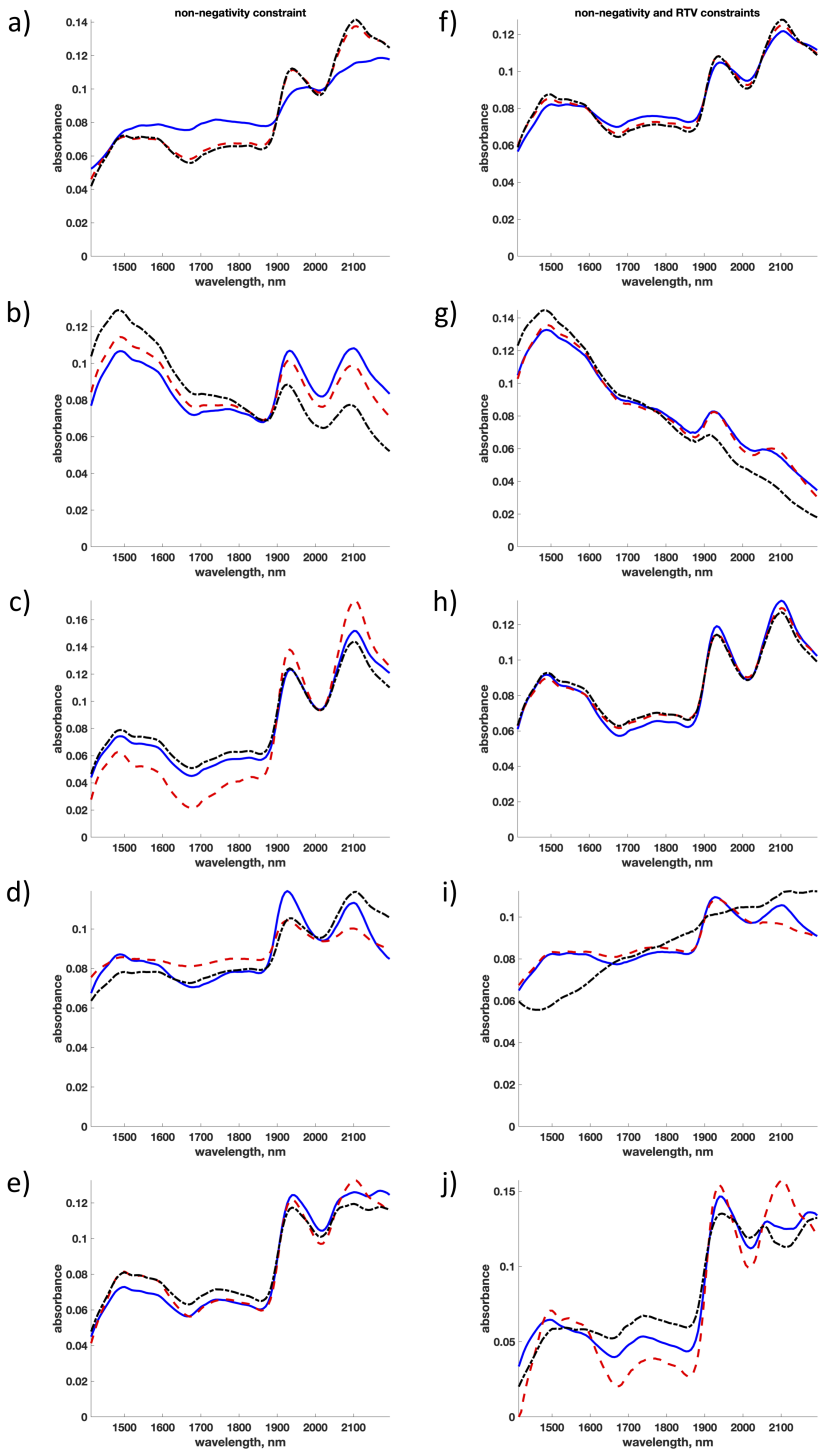


Figure 6 – Cotton/semen data - Resolved spectral profiles obtained by performing a)-e) a standard MCR-ALS decomposition (see Section 2.1) imposing a non-negativity constraint on both $\mathbf{C}$ and $\mathbf{S}^{\mathrm{T}}$ and f)-j) an MCR-ALS decomposition (see Section 2.2) imposing a non-negativity constraint on both $\mathbf{C}$ and $\mathbf{S}^{\mathrm{T}}$ and an RTV constraint on the temporary $\mathbf{C}$ refolded vectors associated to factors #1, #2, #3 and #5 of the three NIR hyperspectral images available (solid blue, dashed red and dashed-dotted black lines). As described in Section 2.3, RTV was applied in an *inverse* fashion for component #2

and, apparently, less scattering-affected spectral signatures were extracted for the purely chemical components underlying the hyperspectral images at hand.

## 5. Acknowledgements

The authors are grateful to Prof. José Manuel Amigo Rubio and Dr. Carolina Santos Silva for having provided the data described and analyzed in this study.

## 6. References

[1] G. Roth, S. Tahiliani, N. Neu-Baker, S. Brenner, Hyperspectral microscopy as an analytical tool for nanomaterials, WIRES Nanomed. Nanobi. 7 (2015) 565–579.
[2] M. Khan, H. Khan, A. Yousaf, K. Khurshid, A. Abbas, Modern trends in hyperspectral image analysis: a review, IEEE Access 6 (2018) 14118–14129.
[3] G. Lu, B. Fei, Medical hyperspectral imaging: a review, J. Biomed. Opt. 19 (2014) 010901.
[4] Å. Rinnan, Pre-processing in vibrational spectroscopy - When, why and how, Anal. Methods 6 (2014) 7124–7129.
[5] Å. Rinnan, F. van den Berg, S. Balling Engelsen, Review of the most common pre-processing techniques for near-infrared spectra, TrAC - Trend. Anal. Chem. 28 (2009) 1201–1222.
[6] B. Debus, R. Vitale, S. Sasaki, T. Asahi, M. Sliwa, C. Ruckebusch, A multivariate curve resolution approach to separate UV-Vis scattering and absorption contributions for organic nanoparticles, Chemometr. Intell. Lab. 160 (2017) 72–76.
[7] C. Ruckebusch (Ed.), Resolving spectral mixtures with applications from ultrafast time-resolved spectroscopy to super-resolution imaging, 1st Edition, Elsevier B.V., 2016.
[8] S. Hugelier, O. Devos, C. Ruckebusch, On the implementation of spatial constraints in Multivariate Curve Resolution Alternating Least Squares for hyperspectral image analysis, J. Chemometr. 29 (2015) 557–561.
[9] S. Hugelier, O. Devos, C. Ruckebusch, Constraining shape smoothness in Multivariate Curve Resolution-Alternating Least Squares, J. Chemometr. 29 (2015) 448–456.
[10] S. Hugelier, O. Devos, C. Ruckebusch, Resolving spectral mixtures with applications from ultrafast time-resolved spectroscopy to super-resolution imaging, 1st Edition, Elsevier B.V., 2016, Ch. A smoothness constraint in Multivariate Curve Resolution-Alternating Least Squares of spectroscopy data, pp. 453–476.
[11] S. Hugelier, S. Piqueras, C. Bedia, A. de Juan, C. Ruckebusch, Application of a sparseness constraint in Multivariate Curve Resolution-Alternating Least Squares, Anal. Chim. Acta 1000 (2018) 100–108.
[12] S. Hugelier, R. Vitale, C. Ruckebusch, Edge-preserving smoothing constraint in Multivariate Curve Resolution-Alternating Least Squares (MCR-ALS) of hyperspectral data, Appl. Spectrosc. 72 (2018) 420–431.
[13] S. Hugelier, P. Firmani, O. Devos, M. Moreau, C. Pierlot, F. Marini, C. Ruckebusch, Weighted fuzzy clustering for (fuzzy) constraints in Multivariate Image Analysis-Alternating Least Square of hyperspectral images, J. Spectral Imaging 5 (2016) a7.
[14] P. Firmani, S. Hugelier, F. Marini, C. Ruckebusch, MCR-ALS of hyperspectral images with spatio-spectral fuzzy clustering constraint, Chemometr. Intell. Lab. 179 (2018) 85–91.
[15] R. Tauler, A. Smilde, B. Kowalski, Selectivity, local rank, three-way data analysis and ambiguity in Multivariate Curve Resolution, J. Chemometr. 9 (1995) 31–58.
[16] R. Tauler, Multivariate Curve Resolution applied to second order data, J. Chemometr. 30 (1995) 133–146.
[17] M. Maeder, Evolving Factor Analysis for the resolution of overlapping chromatographic peaks, Anal. Chem. 59 (1987) 527–530.
[18] W. Windig, J. Guilment, Interactive self-modeling mixture analysis, Anal. Chem. 63 (1991) 1425–1432.
[19] H. Abdollahi, R. Tauler, Uniqueness and rotation ambiguity in Multivariate Curve Resolution methods, Chemometr. Intell. Lab. 108 (2011) 100–111.
[20] A. Golshan, H. Abdollahi, S. Beyramysoltan, M. Maeder, K. Neymeyr, R. Rajkó, M. Sawall, R. Tauler, A review of recent methods for the determination of ranges of feasible solutions resulting from soft modelling analyses of multivariate data, Anal. Chim. Acta 911 (2016) 1–13.

[21] L. Xu, Q. Yan, Y. Xia, J. Jia, Structure extraction from texture via Relative Total Variation, ACM. T. Graphic. 30 (2011) 174:1–174:11.
[22] L. Rudin, S. Osher, E. Fatemi, Nonlinear total variation based noise removal algorithms, Physica D 60 (1992) 259–268.
[23] C. Santos Silva, M. Pimentel, J. Amigo, R. Honorato, C. Pasquini, Detecting semen stains on fabrics using near infrared hyperspectral images and multivariate models, TrAC - Trend. Anal. Chem. 95 (2017) 23–35.
[24] A. de Juan, M. Maeder, T. Hancewitz, R. Tauler, Local rank analysis for exploratory spectroscopic image analysis. Fixed Size Image Window-Evolving Factor Analysis, Chemometr. Intell. Lab. 77 (2005) 64–74.
[25] A. de Juan, M. Maeder, T. Hancewitz, R. Tauler, Use of local rank-based spatial information for resolution of spectroscopic images, J. Chemometr. 22 (2008) 291–298.
[26] A. Savitzky, M. Golay, Smoothing and differentiation of data by simplified least squares procedures, Anal. Chem. 36 (1964) 1627–1639.

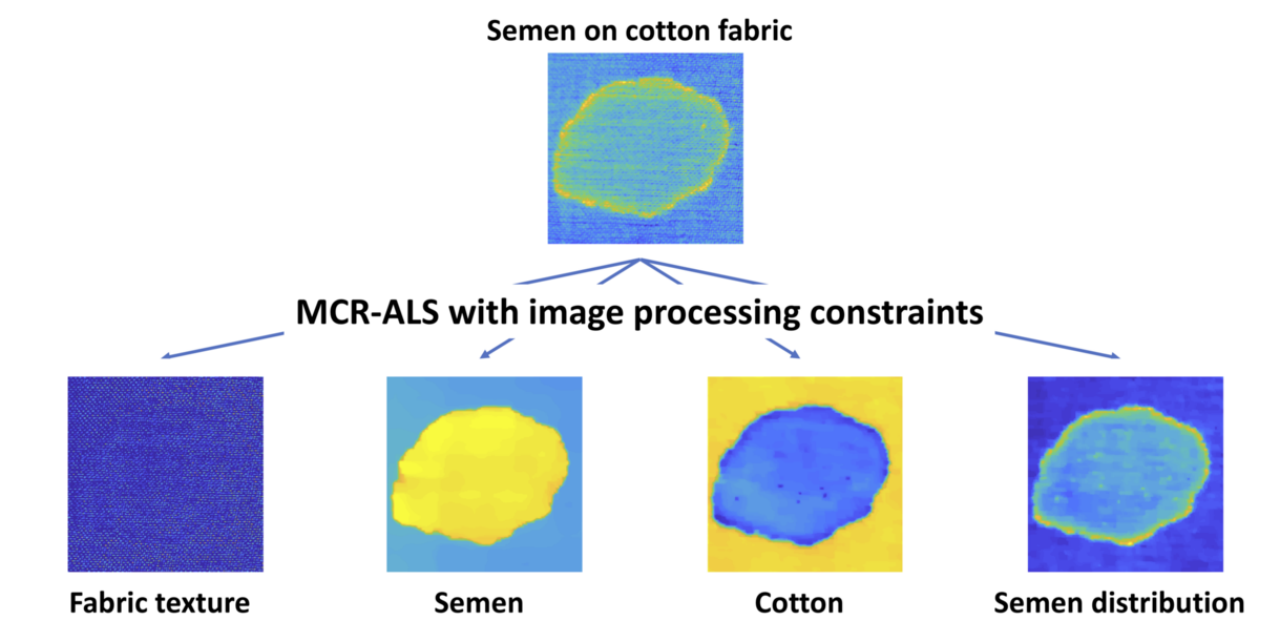
Semen on cotton fabric
MCR-ALS with image processing constraints
Fabric texture
Semen
Cotton
Semen distribution